Object#Oriented Lumped#Parameter Modeling of the Cardiovascular System for Physiological and Pathophysiological Conditions

Citation: Rosalia, L., Ozturk, C., Van Story, D., Horvath, M.A. and Roche, E.T. (2021), Object-Oriented Lumped-Parameter Modeling of the Cardiovascular System for Physiological and Pathophysiological Conditions. Adv. Theory Simul., 4: 2000216.

As Published: http://dx.doi.org/10.1002/adts.202000216

Publisher: Wiley

Persistent URL: https://hdl.handle.net/1721.1/140410

Version: Author's final manuscript: final author's manuscript post peer review, without publisher's formatting or copy editing

Title: Object-oriented lumped-parameter modeling of the cardiovascular system for physiological and pathophysiological conditions.

*Author(s), and Corresponding Author(s)**

*Luca Rosalia, Dr. Caglar Ozturk, David Van Story, Markus A. Horvath, Prof. Ellen T Roche**

*Prof. Ellen T Roche

MIT E25-344, 77 Massachusetts Avenue, Cambridge, MA 02139
E-mail: etr@mit.edu

Keywords: cardiovascular system, lumped-parameter model, Windkessel model, Simscape, object-oriented modeling, pressure-overload heart failure, Fontan circulation

Abstract

In this work, a lumped-parameter Windkessel model of the cardiovascular system that simulates biomechanical parameters of the human physiology is presented. The object-oriented platform provided by the MATLAB-based modeling environment SIMSCAPE is employed to compute blood pressures and flows in each heart chamber and at various sites of the vascular tree. The hydraulic domain allows determination of cardiovascular hemodynamics intuitively from geometrical and mechanical properties of the system, while custom elements model the pumping action of the heart and the effects of respiration on blood flow. The model is validated by comparing predicted hemodynamics with normal physiology during both systole and diastole, demonstrating that changes in arterial pressures with breathing are consistent with reported physiological effects of cardiorespiratory coupling. The capabilities of this platform are explored through two exemplary case studies: (i) pressure-overload heart failure due to aortic constriction, validated *in vitro* and via finite element analysis, and (ii) single-ventricle Fontan physiology, validated *in vitro* and compared with the clinical literature. This platform provides a practical tool for calculation of cardiovascular hemodynamics from hydraulic parameters, enabling intuitive creation of *in silico* representations of complex circulatory loops, planning and optimization of medical interventions, and prediction of clinically relevant patient-specific hemodynamics.

This is the author manuscript accepted for publication and has undergone full peer review but has not been through the copyediting, typesetting, pagination and proofreading process, which may lead to differences between this version and the Version of Record. Please cite this article as doi: 10.1002/adts.202000216.

1. Introduction

The cardiovascular system is a complex network of interdependent elements, whose primary function is to transport oxygen and essential nutrients to tissues in the body. Computational cardiovascular modeling has enabled better comprehension of key physiological mechanisms, improved diagnosis of cardiovascular diseases, and supported development of treatment strategies.[1–4] This approach offers numerous advantages over both *in vitro* and *in vivo* techniques, as it is highly repeatable, cost-effective and non-invasive.[1]

Due to the complex characteristics of the cardiovascular system, analyzing pressures, flows, and volumes over a range of physiological and pathological states constitutes a significant challenge. A broad spectrum of *in silico* simulations have been proposed to represent the boundary conditions of the cardiovascular network, including high- and low-dimensional models. High-dimensional models utilize the finite element approach to provide a comprehensive, multi-scale, and multi-physics description of spatiotemporal hemodynamics as well as of the fluid-structure interactions between the vascular wall and the blood flow in the 2- or 3-D domain.[5,6] However, their implementation necessitates knowledge of several geometrical, mechanical,

and hemodynamic parameters, resulting in elevated computational complexity, which typically limits their application to specific vascular sites and makes them suboptimal in modeling the entire vascular tree. Conversely, low-dimensional models use analytical methods to capture the global properties of the cardiovascular network and are remarkably less computationally intensive rendering them more suitable for hemodynamic simulations of larger portions of the cardiovascular system.[7]

Among low-dimensional *in silico* simulations are lumped-parameter or 0-D models, with the Windkessel representation being the most widely known.[8] Based on the electrical circuit analogy (Ohm's Law), in its simplest form, this consists of a voltage or current source, and of one resistive and one capacitive elements connected in parallel, which correspond to the vascular resistance and compliance respectively. This two-parameter Windkessel description is often expanded into a three-parameter model to include an inductive element connected in series with the resisto-capacitive unit to account for high-frequency effects, thus enhance model accuracy.[9,10] Finally, integration of these blocks into more complex configurations gives rise to multi-compartment models, which allow the represention of the entire vascular network.[11] In the vast majority of these descriptions, each heart

chamber is modeled by an idealized voltage source in series with a time-variant capacitance, effectively representing the cardiac pressure-volume relationship at each heartbeat.[12–14]

Within the cardiovascular realm, multi-compartment lumped-parameter models have served to evaluate several variables in both physiological and disease states, including cardiac output,[15] central aortic pressure,[16] and total peripheral resistance.[17] Furthermore, variations of these models have been implemented to simulate the coronary circulation,[18] congenital heart defects,[19–21] microgravity effects on cardiovascular function,[22] and medical devices for heart failure[23–25] or other conditions.[26,27] However, current 0-D descriptions remain decoupled from the geometrical and mechanical behavior of the network they represent, and are therefore often replaced by, or integrated with, hydraulic benchtop systems or mock circulatory loops for experimental studies and device testing. These consist of a pulsatile pump, tubes, and compliance chambers, and are commonly used in cardiovascular research due to their versatility and low cost.[28–33] Nevertheless, these systems are limited to simplified representations of the cardiovascular network and building an *in vitro* model of the entire vascular tree remains challenging.[34]

Despite the ability to capture the general shape of pressure waveforms with low computational demand, the clinical applicability of lumped-parameter representations is improved when these models can reproduce patient-specific cardiovascular flow conditions [35–37] this emphasizing the need for patient-specific models, which are clinically relevant, yet do not necessitate invasive measurements.[38] This specificity is extremely challenging in the context of electrical-based Windkessel models, as they require pressure and flow measurements to estimate the values of their constituting resistive, capacitive, and inductive elements. Although emerging technologies including 4-D flow MRI have shown promise in obviating this problem, the associated costs significantly limit their application.[38]

Object-oriented 0-D models in the hydraulic domain have the potential to bridge the gap between electrical analog representations that lack geometrical and mechanical effects, and the practical simplifications required to build a flow loop *in vitro*.[39] Analytical solutions that couple simplified Navier-Stokes equations with the traditional elements of the Windkessel model have been recently formulated and validated.[39,40] These studies suggest that, in addition to enabling intuitive *in silico* representations of *in vitro* models of various complexities, where the physical properties of the

components are known, hydraulic analog models could reduce the invasiveness of the procedures required for the formulation of patient-specific lumped-parameter models. Therefore, they offer several potential benefits to clinical practice and cardiovascular biomechanics research.

In this work, we propose an object-oriented lumped-parameter model of the cardiovascular network in the hydraulic domain, where hemodynamics are primarily defined by the geometrical and mechanical characteristics of the human physiology. We adopt the object-oriented platform provided by the MATLAB-based modeling environment SIMSCAPE, and utilize the *Hydraulic* library, which we expand to mimic cardiac contraction and the effects of respiration on blood flow. General cardiovascular hemodynamics are then presented as a general validation of the proposed model. The capabilities of the model are further investigated through hemodynamic analysis of two disparate clinically-relevant scenarios, namely (i) pressure-overload heart failure due to aortic constriction, validated both experimentally and via finite element analysis (FEA), and (ii) the Fontan circulation in patients with surgically corrected hypoplastic left heart syndrome, analogously validated *in vitro* and compared with findings from a recent clinical study.

2. Simulation approach

2.1. SIMSCAPE environment

Object-oriented modeling allows to create *in silico* representations of a system by assembling domain-specific physical components into a network.[41] The proposed hydraulic model of the cardiovascular system was built on the MATLAB-based SIMSCAPE environment, which uses the default ODE 23t implicit solver. This platform has been previously used to simulate Windkessel models of various complexities as equivalent electrical circuits.[14] However, it was never explored in the hydraulic domain, which may offer several advantages when the geometrical and material properties of the system to be represented are known.

2.1.1. Elements used

The components of the default SIMSCAPE *Hydraulic* library alone are sufficient to recreate a simple representation the cardiovascular system. However, these elements do not allow modeling of cardiac contractility using the time-varying elastance description most commonly adopted in the literature.[42–44] Furthermore, the standard library does not account for important physiological phenomena including the effects of respiration on blood pressures and flows. For this reason, we developed the *Cardiovascular* library to introduce a custom variable-compliance compliance

chamber element. The main blocks utilized in this simulation are represented in **Figure 1a** and described below.

Hydraulic pipeline: This is a composite element, which accounts for frictional pressure losses as well as wall compliance and fluid compressibility. The pressure loss of the pipeline is calculated under steady-state momentum and fully-developed conditions by the Darcy-Weisbach law in **Equation 1**:

$$p_L = f\frac{L+L_{eq}}{D}\frac{\rho}{2A^2}q|q| \quad (1)$$

where f is the friction factor, which depends on the flow regime, L is the pipe length, L_{eq} represents the aggregate equivalent length of local resistances due to bends, inlet, or outlet losses, D is the hydraulic diameter of the pipe, A is the cross-sectional area, ρ is the fluid density, and q the volumetric flow rate through the tube, which is positive when the pressure at the inlet is greater than that at the outlet. Wall compliance must be provided as an input parameter K_p, indicated as a change in the wall internal diameter d per unit pressure change P. The relationship between these variables can be expressed in the Laplace domain in **Equation 2**:

$$d(s) = \frac{K_p}{1+\tau s}\,P(s) \quad (2)$$

where τ is the time constant which captures the time-dependent response of viscoelastic materials and s is the Laplace operator. The order of magnitude of K_p was estimated from the pipeline geometry and the corresponding compliance values in the lumped-parameter literature (see Supplementary Information). Finally, fluid compressibility is calculated from the bulk modulus of the medium. Despite having a negligible effect on cardiovascular hemodynamics, in this simulation, a value for the bulk modulus must be provided to satisfy the equations in the hydraulic domain.

Constant volume hydraulic chamber: This element captures the same effects due to wall compliance (**Equation 2)** without taking into account frictional losses.

Variable-compliance compliance chamber: Based on the constant volume hydraulic chamber element, this custom block takes wall compliance values K_p as a time-dependent input signal. This element was therefore introduced as part of the *Cardiovascular* library to simulate contractility of each of the four heart chambers. A simple approximation of the well-known time-varying elastance models was used to define ventricular compliance,[42–44] while atrial compliance was computed from the existing experimental literature[45] (**Figure S1**). Furthermore, this element enabled modeling of the compliance of the vascular bed in the abdominal and pulmonary cavities as they vary during the breathing cycle.[46,47]

Linear hydraulic resistance: This is to define an overall hydraulic resistance at a given site of the network, which does not depend upon the geometrical or mechanical characteristics of the physical system. The pressure loss computed by this block is directly proportional to the flow rate, with resistance being the proportionality constant. This is analogous to the resistors used in the electrical-domain Windkessel model, and it enables modeling of the resistance to flow when geometrical information is not available.

Centrifugal pump: Supplies energy to the hydraulic network. This block is connected to a hydraulic reference and receives the rotational speed of the driving shaft as an input. This is defined by the user to generate the desired input pressure to the system.

Check valve: This is a type of valve which allows flow in one direction only. When time-dependent effects are neglected, the valve opens linearly to the maximum opening area. First-order opening dynamics could be modeled if a time constant is defined. In the electrical domain, these elements correspond to diodes, preventing backflow from the great arteries into the ventricles, and

from the ventricles into the atria.[48–53] Conversely, elimination of this valve could be used to model several pathological conditions, including valvular insufficiency or regurgitation.

Variable area hydraulic orifice: This valve permits to model the pressure drop across an orifice of cross-sectional area, that is defined as an input signal to the block. The flow rate q through the orifice is directly proportional to the flow discharge coefficiend C_D and the cross-sectional area A, and depends upon the fluid density ρ, the pressure drop p, and the critical pressure p_{cr} at which the laminar-to-turbulent regime transition occurs (**Equation 3)**:

$$q = C_D\, A \sqrt{\frac{2}{\rho}}\, \frac{p}{(p^2+p_{cr}^2)^{\frac{1}{4}}} \qquad (3)$$

Custom hydraulic fluid: Fluid properties including density, kinematic viscosity, and bulk modulus can be defined using this block. This block provides an additional advantage over traditional electrical analog models by enabling tuning of the properties of blood, and therefore simulations of cardiovascular hemodynamics resulting from blood disorders such as hyperviscosity syndrome - a common sequela of hematologic malignancies. Moreover, by allowing changes of the mechanical properties of the medium, our platform is particularly suited for modeling mock circulatory loops, often adopting media with various densities and viscosities.

Further details about these elements can be found in the Supporting Information.

2.2. Full heart model

The full heart model proposed in this work is composed of a geometric approximation of each cardiac chamber as well as a hybrid description of the systemic and pulmonary circulations, constituting a combination of linear resistances and geometric elements.

Each cardiac chamber, namely left and right ventricles and left and right atria, consists of a hydraulic pipeline modeling the resistance to flow, and of a variable-compliance compliance chamber simulating the contractile and relaxation characteristics of the heart. Each chamber is approximated to a cylindrical shape of fixed length and variable diameter, that is defined by its relationship with pressure and compliance in Equation 2. Heart valves, including the aortic, pulmonary, mitral, and tricuspid valves are located at their respective anatomical sites and modeled via a variable-area orifice, connected in series with a unidirectional check valve to prevent backflow. In addition to these elements, the left ventricle incorporates a centrifugal pump that defines the pulsatile pressure supplied to the network, as well as a custom hydraulic fluid block defining the mechanical properties of the fluid, i.e. blood.

An illustration of the network is depicted in Figure 1b, while the simulation schematic is shown in Figure 1c. The systemic circulation begins with the aorta, which is divided into ascending, descending, and thoracic segments, with the upper body circulation stemming from the intersection between the two proximal sections, and the abdominal and lower body vasculatures originating in parallel, both distal to the thoracic aorta. The abdominal and lower body compartments rejoin at the abdominal portion of the inferior vena cava. The thoracic vena cava terminates into the right atrium, in liaison with the superior vena cava arising from the upper body circulation. The pulmonary circulation completes the loop linking the right ventricle to the left atrium.

In this representation, the majority of the elements are defined by their geometry and mechanical properties: each heart chamber, the aorta, the pulmonary artery, and the superior and inferior venae cavae are all characterized by values of length and initial diameter reported in the literature, as well as by their compliance and other mechanical properties, including surface roughness and viscoelastic time constant, which have been estimated. In addition, each heart valve is associated with their respective orifice area. Other portions of the upper, abdominal, lower, and abdominal

compartments are modeled using a combination of two linear hydraulic resistive elements and one compliance chamber. Similar to the resistors of the electrical Windkessel model, the resistive elements are entirely defined by a constant representing the resistance to flow, and thus require no geometrical or mechanical information. For each compartment, two elements model the arterial and venous resistances, as previously described in the literature.[22] Furthermore, there is a compliance chamber between each pair of hydraulic resistors. The geometry of each of these chambers was calculated from reported values of the blood volume, and their compliance was estimated. The main input parameters of the proposed simulation are summarized in Table 1, while a more comprehensive set of parameters can be found in Table S1.

3. Results

3.1 Full heart hemodynamics

Our results demonstrate the ability of the proposed model to recapitulate physiologic hemodynamics (Table 2). The pressure-volume (PV) relationships relative to each cardiac chamber closely mimic those observed in normal

physiology.[54] The pressure and volume waveforms, as well as the PV loops for the left and right ventricles and for the left atrium are illustrated in Figure 2.

As anticipated, the systolic pressure in the left heart largely exceeds that generated by the right ventricle (Figure 2a). Furthermore, unlike the left ventricular PV loop, which is characterized by prominent isovolumetric contraction and relaxation phases, the right ventricular PV loop exhibits a more triangular shape (Figure 2b). This occurs as the right ventricular ejection into the pulmonary artery commences at lower pressures and earlier into the cardiac cycle compared to the left side of the heart. The stroke volume, i.e. the difference between the volume at end diastole and end systole, is similar in the right as in the left ventricles, and within normal range. This is a key hemodynamic parameter in that, together with the heart rate, it determines the cardiac output, that is the amount of blood pumped though the circulatory system every minute. Finally, the characteristic bump corresponding to atrial contraction is observed along the left ventricular end-diastolic PV relationship prior to systole (Figure 2b).

Both the left and right PV loops are distinguished by the presence of two prominent peaks. The left atrial pressure and volume tracings and PV loop

are shown in Figure 2c-d. The right atrial pressure and volume tracings and PV loop can be found in Figure S2. The atrial PV loop begins with a rapid and almost linear increase in pressure with volume, corresponding to the atrial filling phase. This transitions into the pressure and volume drops caused by passive emptying, followed by a second peak in pressure due to atrial contraction, which completes the loop. The right and left atrial PV loops are very similar in shape, with lower pressures often being exhibited in the right heart.

The aortic and pulmonary pressures were also observed to evaluate the accuracy of the model and are shown in Figure 2a. As predicted, the aortic pressure closely follows that of the left ventricle during systole and slowly decays upon aortic valve closure during diastole. Similarly, the pulmonary artery pressure closely follows that of the right ventricle during systole. However, decay dynamics are markedly different between the aorta and pulmonary artery, due to the lower pressure and the prolonged ejection characteristic of the right heart.

3.1.3 Respiratory effects on arterial pressure

Hemodynamics changes due to breathing were modeled by replacing the compliance chambers of the abdominal and thoracic compartments with their time-varying analogous from the *Cardiovascular* library. Compliances were calculated based on the inverse proportionality between compliance and pressure (**Equation 2**). Therefore, compliance was set to increase during inspiration and drop during expiration in the thoracic cavity, and vice versa in the abdominal space, as shown in **Figure 3a-b**. Results are consistent with what has been observed physiologically.[54] **Figure 3c** illustrates that both the systolic and diastolic arterial pressures decrease during inspiration as a result of enhanced venous return and increase during expiration.

The ability to include the effects of respiration on cardiovascular hemodynamics allows the proposed platform to model medical conditions where the interdependency between the cardiovascular and respiratory system plays a critical role. An example is that of patients with single ventricle physiology following the Fontan procedure, as described later.

3.2. Case study 1: Aortic Constriction

3.2.1 Motivation and model description

The aorta is the main and largest artery of the body as it originates directly from the heart and carries blood to the peripheral circulation. Alterations in its geometry or mechanical properties are known to affect local hemodynamics, ultimately driving disease, including plaque formation, aortic aneurysm and dissection.[55,56] Due to the mechanical and hemodynamic

coupling with the left ventricle, a partially occluded, constricted, or stiffened aorta causes an increase in the force required for ejection, which may ultimately lead to heart failure. Clinically, the pressure difference between the left ventricle and aorta in systole - the transaortic pressure gradient - serves as an indication of disease severity.[57,58]

To capture the relationship between aortic constriction (AC) and transaortic gradient, we readapted our simulation by splitting the ascending aorta into two segments: the more proximal, of length l = 2 cm, to mimic local constriction through a reduction in cross-sectional area and reduced compliance, and the more distal one that represents the remaining portion of the vessel. The aortic and left ventricular hemodynamics were calculated at steady state for cross-sectional reductions of AC = 45, 60, 80, 85, 90%.

3.2.2 *In vitro* validation

A simple flow loop system was built to validate the *in silico* results on a benchtop (**Figure S3)**. A pulsatile pump (Pulsatile Blood Pump 55-3305, Harvard Apparatus) was employed to draw water from a reservoir at a rate of 60 beats per minute (bpm) with a stroke volume of 79 mL, from the computational model. Two adjustable resisto-capacitive pairs, each consisting of a compliance chamber and a resistive valve, were connected in series to the pump, across a low modulus latex

rubber tube (E ≈ 1.4 MPa, d_{in} = 3/4", d_{out} = 7/8", McMaster-Carr) similar to the ascending aorta in both the geometry and tensile mechanical properties (E = 1.18 ± 0.21 MPa)[59]. These pairs allow control of compliance and resistance of both the arterial and venous systems. They were adjusted to replicate the baseline systolic and diastolic aortic pressures obtained *in silico*, as measured using PASCO wireless pressure sensors across the mock vessel.

AC was achieved using a simple electromechanical constriction device, illustrated in **Figure 4a**. This is composed of an Arduino-controlled non-captive stepper motor (Nema 11 0.75A Lead 2mm/0.07874", STEPPERONLINE) to gradually compress the aorta. A custom case was 3D-printed to house the motor and provide a secure attachment to the wall of the mock aorta. We utilized a circular nut plate of diameter d = 2 cm to reproduce the length of the most proximal aortic segment of the *in silico* model. A semi-rigid wireless endoscopic camera (1080P HD, 30 fps, NIDAGE) was inserted to capture images of the cross-sectional area at AC values similar to those of the computational model and track changes, then post-processed using the MATLAB image processing toolbox and matched with the corresponding pressure readings. Images of the aorta at AC ≈ 0%, 50%, and 85% are provided in **Figure 4b**.

3.2.3 FEA analysis

Finite element analysis (FEA) was employed to analyze the mechanical and hemodynamic changes induced by AC and validate our results. For this purpose, we utilized the four chamber FE dynamic heart model (Living Heart Model – LHM) on Abaqus 2018 software (Simulia, Dassault Company).[60] This model was constructed from cardiac MRI data[61], thus it provides an accurate representation of the human anatomy. The LHM consists of multi-physics models of the electro-mechanical cardiac response, structural deformations, and fluid cavity-based hemodynamics. In the

first step, the electro-mechanical simulation analyzes the excitation and contraction characteristics of the heart during the cardiac cycle. In a subsequent step, coupling of structural deformation with the hemodynamic model through the Abaqus/Explicit solver scheme allows simulation of the motion dynamics and cardiac function. The blood flow model was implemented using surface-based fluid cavities. The flow exchange profiles were defined between the fluid cavities based on a 0-D lumped parameter model,[60] with seven viscous resistances and three capacitive elements used to represent the heart motion as associated with compliance and flow dynamics. Further information on the blood flow model can be found in **Figure S4**.

AC was simulated on FEA using a circular plate (d = 2 cm) attached to the shaft of a linear actuator, as in **Figure 4c**, and linear travel was applied to the contact plate of the end-effector. Simulations were run for six different values of AC similar to those employed above, and three full cardiac cycles were simulated for each AC to achieve steady-state (**Figure 4d**). The total element count of the FE model was approximately 210,000 (linear tetrahedral elements).

3.2.4 Aortic constriction results

Results from the simulation, *in vitro* validation, and FEA modeling demonstrate that AC leads to an increase in the left ventricular and a drop in the aortic pressures, effectively establishing a gradient. Under ideal conditions, this result can be intuitively thought of as a direct application of the continuity and Bernoulli's equations, which together describe the relationship between the cross-sectional area of a pipe and the kinetic energy associated with flow alongside other parameters. At these sites, the pressure changes are illustrated in **Figure 4e** under normal conditions, and in **Figure 4f** at AC = 85%, which shows a maximum, or systolic, transaortic pressure gradient of approximately 6 mmHg. The pressure gradient was observed to follow an exponential trend consistently across the *in silico* (R^2 = 0.8965), *in vitro* (R^2 = 0.9788 ± 0.0027, N = 3), and FEA (R^2

= 0.8875) platforms, rapidly growing for constrictions of greater than 80% (**Figure 4g**). The magnitude of the gradient obtained *in silico* is slightly lower than that calculated experimentally and via FEA. This discrepancy could be due to the idealized hemodynamics of the lumped-parameter model, where the constricted aorta preserves its original circular cross-section, as well as limitations of the FEA approach, including simplified resistance and compliance elements, boundary conditions, and meshing quality, as further outlined in the Discussion section below.

The left ventricular PV hemodynamics obtained with the proposed lumped-parameter model and on FEA at AC = 0 and 85% are illustrated in **Figure 4h**. The left ventricular PV loops show excellent agreement, with elevated systolic left ventricular pressures upon AC. Moreover, a reduction in the left ventricular end-systolic volume and the stroke volume, albeit minor, was captured by the proposed lumped-parameter platform. This is a consequence of an elevated aortic resistance (or arterial elastance) and is clinically observed in a variety of diseases including aortic stenosis and atherosclerosis.

3.3. Case study 2: Fontan hemodynamics

3.3.1 Motivation and model description

Hypoplastic left heart syndrome is a form of univentricular congenital heart disease in which the left side of the heart is underdeveloped, thus unable to pump blood to the body adequately. In these patients, a series of surgeries are required to restore blood flow. The last of these procedures is the Fontan operation, which is performed to shunt venous blood from the body directly to the pulmonary circulation, bypassing the heart.[62] Although this surgery prolongs life, hemodynamic abnormalities result from this procedure, and the resulting single ventricle physiology, including low

pulsatile flow within the inferior vena cava (IVC) and elevated hepatic venous pressures, which can lead to a host of long-term morbidities and mortality.[63–66]

In this case study, we present a lumped-parameter representation of the Fontan circulation to illustrate the role that respiration alone plays on the hemodynamics of venous return, as recently demonstrated *in vivo*.[66] This work concluded that breathing, rather than the pumping action of the heart, is responsible for the flow characteristics observed in the IVC in this patient population. By comparing the IVC hemodynamics obtained *in silico*, we aim to further demonstrate the versatility of our proposed platform.

The simulation network was readapted to emulate the Fontan anatomy. As shown in **Figure 5a**, the heart was simulted by one ventricle and one atrium, with a shunt connecting the IVC to the superior vena cava (SVC) and the pulmonary circulation. In this description, breathing was simulated via variable-compliance chambers, in a similar fashion to our previous simulations. Furthermore, a constant input was provided to the centrifugal pump and the heart valves ere removed from the model to eliminate any time-dependent effect from the beating of the heart. By matching the average respiratory rate and cardiac output of the patient population in the clinical study, we closely replicated the breathing gating analysis.[66] The geometrical characteristics of the heart chambers were modified from the baseline simulation to more accurately reproduce cardiac anatomy in hypoplastic left heart syndrome. Finally, the thoracic IVC was replaced with a simulated Dacron shunt to mimic that typically implanted during the surgical procedure,[67,68] and pulmonary resistances were increased to model pulmonary hypertension, which is highly prevalent in Fontan patients.[69] The input parameters of this model and the schematic can be found in **Table S2** and **Figure S5** respectively.

3.3.2 Experimental set-up

We further validated the results of the *in silico* model using a benchtop simulator of Fontan hemodynamics recently developed by our group.[70] This system consists of a mock circulatory loop integrated with a soft-actuated synthetic diaphragm to mimic breathing (**Figure 5b**). Diaphragmatic motion generates physiological pressures in both the thoracic and abdominal cavities as demonstrated in our previous work.[71] For this study, we employed our benchtop simulator to investigate IVC hemodynamics at a respiratory rate and cardiac output that are similar to those of the *in vivo* study as well as of the proposed simulation. A constant pressure head reservoir was used to provide a constant input to the system, while respiratory pressures and IVC hemodynamics were recorded throughout each breathing cycle using pressure sensors (ArgoTrans model2, Argon Medical Devices) and a flowmeter (Transonics Inc. 28PAU).

3.3.3 Fontan hemodynamics results

Figure 5c illustrates the IVC flow during a breathing cycle beginning at inspiration. Results from the *in silico* model closely match those from the clinical study of reference and from our benchtop simulator. IVC flow is seen to increase during inspiration and drop during expiration. We computed a mean IVC pressure of 18.5 mmHg on our simulation, which very closely matched that measured on the benchtop simulator. Furthermore, the peak IVC was similar across our platforms, as summarized in **Table 3.**

4. Discussion

In this work, we present a Windkessel lumped-parameter model that is based on the anatomy and biomechanics of the human cardiovascular system. This was developed using the object-oriented MATLAB-based SIMSCAPE platform in the hydraulic domain. A custom variable-compliance element was integrated to mimic cardiac contractility and compliance variations due to respiration. The model was constructed using the geometrical and mechanical characteristics of the cardiovascular anatomy, whereas values for local resistances were adopted from the literature when it was impractical to geometrically represent the network at various sites of the cardiovascular tree. The efficiency of traditional electrical analog lumped-parameter models and the physical intuitiveness and practical advantage associated with the hydraulic domain coalesce in the platform. This makes the proposed model suitable for creating intuitive representations of *in vitro* hydraulic mock circulatory loops, informing device development through the optimization of the associated geometry and material properties, and predicting patient-specific hemodynamics of clinical relevance.

This model closely replicates the cardiovascular hemodynamics within the physiological range in both the systolic and diastolic phases of the cardiac

cycle, and has numerous advantages over previously reported work. In addition to ventricular PV loops, we were able to reproduce atrial PV loops, which are not commonly reported for Windkessel models. Furthermore, this platform predicts the effects of breathing on arterial pressure - a decrease during inspiration and increase during expiration.

A major advantage of our proposed simulation over the traditional Windkessel representation is the ability to recapitulate the effects of geometrical and mechanical abnormalities of large vessels. This enables prediction of changes in the left ventricular pressures and volume caused by aortic constriction and stiffening, which we validated using a simple *in vitro* mock circulatory loop and FEA. Results consistently showed that the transaortic pressure gradient increases in an exponential fashion with reductions in the aortic luminal area - a clinically relevant prediction given that changes in the afterload can lead to heart failure. Simulation of the effects of respiration on Fontan hemodynamics further demonstrated the versatility of the proposed platform, which was readapted to the univentricular heart anatomy. Our *in silico* results accurately replicated a recent *in vivo* study,[66] and was validated *in vitro* using our cardiopulmonary benchtop simulator. We found that, at the same respiratory rate and cardiac

output, the IVC pressure and flow characteristics were similar across the three platforms.

However, some limitations associated with our model should be considered. First, the central venous pressure (CVP), is skewed towards the upper limit of the physiological range. Although higher compliance values in the right ventricle lower the computed CVP, the simulation becomes less stable and the time required to reach steady-state increases dramatically. Moreover, the simulation does not include inertial elements that would capture the high-frequency pressure changes associated with higher-order velocity changes.

In addition, although our platform accurately predicted the physiologic decrease in arterial pressure at inspiration and increase at expiration, several mechanisms that contribute to this phenomenon have been omitted for simplicity. For instance, no respiration-driven compliance changes were considered for large vessels such as the aorta, IVC, SVC, and pulmonary artery, as well as for any of the cardiac chambers, particularly of the right heart, as they are affected by respiratory mechanics. Furthermore, changes in the heart rate, as well as the mechanical interaction between the right and left ventricle, which causes a reduction in left ventricular filling during

inspiration, thus a decline in systolic blood pressure, could not be accounted for in this simulation, as these go beyond the capabilities of lumped-parameter models.

Finally, differences between our lumped-parameter model and the FEA simulation should be mentioned to explain why pressure changes induced by AC were marginally higher when predicted by FEA compared to our lumped-parameter platform. In FEA, discretization errors associated with meshing quality, use of simplified Windkessel elements to define flow exhange between different fluid cavities, and turbulent flow at the cardiac wall may result in additional vicous and frictional losses. These could be responsible for a transaortic pressure gradient that is greater in FEA than what is predicted by our lumped-parameter model and observed experimentally.

5. Conclusions

The proposed work constitutes an object-oriented lumped-parameter representation of the cardiovascular system in the hydraulic domain, based on the geometrical and biomechanical characteristics of the network. Results show that this model closely mimics the hemodynamics of normal physiology

and that the effects of breathing on cardiovascular hemodynamics could be successfully simulated. Two case studies showcased the versatility and advantage of this model over conventional approaches.

Future work will first focus on exploiting the capabilities of this model by simulating a wider spectrum of cardiovascular and respiratory conditions. Second, respiratory mechanics could be optimized via modeling of breathing-driven compliance changes of the heart chambers and other large vessels. Finally, inertial elements could be included to capture the high-frequency response of the system due to higher-order velocity changes, when relevant for a given application, albeit at the expense of computational efficiency.

In conclusion, the presented platform offers a physically-intuitive approach to modeling the cardiovascular system. This can enable the development of *in silico* models that closely replicate the mock circulatory loops commonly used in cardiovascular research and investigate more complex systems which would be impractical to replicate *in vitro*. Finally, by representing disease-specific anatomies, this model may have utility as a user-friendly and computationally efficient tool to better understand cardiovascular hemodynamics and the effect of intervention on cardiac function.

Supporting Information

Supporting Information is available from the Wiley Online Library or from the author.

Acknowledgements

We acknowledge funding from the Harvard-Massachusetts Institute of Technology Health Sciences and Technology program, the SITA Foundation Award from the Institute for Medical Engineering and Science, and the Charles H. Hood Foundation Award for Excellence in Child Health.

Received: ((will be filled in by the editorial staff))

Revised: ((will be filled in by the editorial staff))

Published online: ((will be filled in by the editorial staff))

References

[1] B. Owen, N. Bojdo, A. Jivkov, B. Keavney, A. Revell, *Biomech. Model. Mechanobiol.* **2018**.

[2] A. Quarteroni, L. Formaggia, *Handb. Numer. Anal.* **2004**.

[3] A. Quarteroni, A. Manzoni, C. Vergara, *Acta Numer.* **2017**.

[4] M. Capoccia, S. Marconi, S. A. Singh, D. M. Pisanelli, C. De Lazzari, *Biomed. Eng. Online* **2018**.

[5] A. Lopez-Perez, R. Sebastian, J. M. Ferrero, *Biomed. Eng. Online* **2015**.

[6] X. Xie, M. Zheng, D. Wen, Y. Li, S. Xie, *Biomed. Eng. Online* **2018**.

[7] S. Zhou, L. Xu, L. Hao, H. Xiao, Y. Yao, L. Qi, Y. Yao, *Biomed. Eng. Online* **2019**.

[8] K. Sagawa, R. K. Lie, J. Schaefer, *J. Mol. Cell. Cardiol.* **1990**.

[9] K. H. Wesseling, J. R. C. Jansen, J. J. Settels, J. J. Schreuder, *J. Appl. Physiol.* **1993**.

[10] N. Stergiopulos, B. E. Westerhof, N. Westerhof, *Am. J. Physiol. - Hear. Circ. Physiol.* **1999**.

[11] A. C. Guyton, T. G. Coleman, H. J. Granger, *Annu. Rev. Physiol.* **1972**.

[12] G. Avanzolini, P. Barbini, A. Cappello, A. Cevese, *IEEE Trans. Biomed. Eng.* **1985**.

[13] Y. Sun, M. Beshara, R. J. Lucariello, S. A. Chiaramida, *Am. J. Physiol. - Hear. Circ. Physiol.* **1997**.

[14] J. Fernandez de Canete, P. del Saz-Orozco, D. Moreno-Boza, E. Duran-Venegas, *Comput. Biol. Med.* **2013**.

[15] R. B. P. de Wilde, J. J. Schreuder, P. C. M. van den Berg, J. R. C. Jansen, *Anaesthesia* **2007**.

[16] S. Vennin, Y. Li, M. Willemet, H. Fok, H. Gu, P. Charlton, J. Alastruey, P. Chowienczyk, *Hypertension* **2017**.

[17] T. A. Parlikar, T. Heldt, G. V. Ranade, G. C. Verghese, in *Comput. Cardiol.*, **2007**.

[18] Z. Duanmu, M. Yin, X. Fan, X. Yang, X. Luo, *Sci. Rep.* **2018**.

[19] E. Kung, G. Pennati, F. Migliavacca, T. Y. Hsia, R. Figliola, A. Marsden, A. Giardini, M. Investigators, *J. Biomech. Eng.* **2014**.

[20] D. E. Schiavazzi, A. Baretta, G. Pennati, T. Y. Hsia, A. L. Marsden, *Int. j. numer. method. biomed. eng.* **2017**.

[21] S. Shimizu, D. Une, T. Kawada, Y. Hayama, A. Kamiya, T. Shishido, M. Sugimachi, *J. Physiol. Sci.* **2018**.

[22] T. Heldt, E. B. Shim, R. D. Kamm, R. G. Mark, Massachusetts, *J. Appl. Physiol.* **2002**.

[23] F. Scardulla, V. Agnese, G. Romano, G. Di Gesaro, S. Sciacca, D. Bellavia, F. Clemenza, M. Pilato, S. Pasta, *Cardiovasc. Eng. Technol.* **2018**.

[24] M. Granegger, H. Dave, W. Knirsch, B. Thamsen, M. Schweiger, M. Hübler, *Cardiovasc. Eng.*

Technol. **2019**, *10*, 69.

[25] D. Burkhoff, M. S. Maurer, S. M. Joseph, J. G. Rogers, E. Y. Birati, J. E. Rame, S. J. Shah, *JACC Hear. Fail.* **2015**, *3*, 275.

[26] M. Abdi, A. Karimi, M. Navidbakhsh, G. Pirzad Jahromi, K. Hassani, *Int. J. Numer. Model. Electron. Networks, Devices Fields* **2015**.

[27] K. Pekkan, D. Frakes, D. De Zelicourt, C. W. Lucas, W. J. Parks, A. P. Yoganathan, in *ASAIO J.*, **2005**.

[28] N. Westerhof, G. Elzinga, P. Sipkema, *J. Appl. Physiol.* **1971**.

[29] S. C. Koenig, G. M. Pantalos, K. J. Gillars, D. L. Ewert, K. N. Litwak, S. W. Etoch, *ASAIO J.* **2004**.

[30] G. G.A., C. R., G. J.S., E. D.L., S. M.A., S. M.S., K. S.C., *ASAIO J.* **2012**.

[31] P. A. Midha, V. Raghav, I. Okafor, A. P. Yoganathan, *Ann. Biomed. Eng.* **2017**.

[32] Y. Wang, S. C. Koenig, M. A. Sobieski, M. S. Slaughter, G. A. Giridharan, *Cardiovasc. Eng. Technol.* **2017**.

[33] A. Petrou, M. Granegger, M. Meboldt, M. S. Daners, *ASAIO J.* **2019**.

[34] J. Gehron, J. Zirbes, M. Bongert, S. Schäfer, M. Fiebich, G. Krombach, A. Böning, P. Grieshaber, *ASAIO J.* **2019**.

[35] K. Sughimoto, F. Liang, Y. Takahara, K. Mogi, K. Yamazaki, S. Takagi, H. Liu, *J. Thorac. Cardiovasc. Surg.* **2013**.

[36] Z. Keshavarz-Motamed, J. Garcia, E. Gaillard, R. Capoulade, F. Le Ven, G. Cloutier, L. Kadem, P. Pibarot, *PLoS One* **2014**.

[37] S. Pant, C. Corsini, C. Baker, T. Y. Hsia, G. Pennati, I. E. Vignon-Clementel, *J. Biomech.* **2016**.

[38] B. Casas, J. Lantz, F. Viola, G. Cedersund, A. F. Bolger, C. J. Carlhäll, M. Karlsson, T. Ebbers, *Sci. Rep.* **2017**.

[39] Y. Aboelkassem, Z. Virag, *J. Theor. Biol.* **2019**.

[40] Y. Aboelkassem, D. Savic, S. G. Campbell, *J. Theor. Biol.* **2015**.

[41] G. Zauner, D. Leitner, F. Breitenecker, in *EOOLT 2007 - Proc. 1st Int. Work. Equation-Based Object-Oriented Lang. Tools, Conjunction with ECOOP 2007*, **2007**.

[42] H. Suga, K. Sagawa, A. A. Shoukas, *Circ. Res.* **1973**.

[43] H. Suga, K. Sagawa, *Circ. Res.* **1974**.

[44] H. Suga, K. Sagawa, D. P. Kostiuk, *Cardiovasc. Res.* **1976**.

[45] B. D. Hoit, Y. Shao, M. Gabel, R. A. Walsh, *Circulation* **1994**.

[46] B. J. Kimura, R. Dalugdugan, G. W. Gilcrease, J. N. Phan, B. K. Showalter, T. Wolfson, *Eur. J. Echocardiogr.* **2011**.

[47] L. Bodson, A. Vieillard-Baron, *Crit. Care* **2012**.

[48] E. B. Shim, C. H. Leem, Y. Abe, A. Noma, in *Philos. Trans. R. Soc. A Math. Phys. Eng. Sci.*, **2006**.

[49] Y. S. Kim, E.-H. Kim, H.-G. Kim, E. B. Shim, K.-S. Song, K. M. Lim, *Integr. Med. Res.* **2016**.

[50] Y. Shi, P. Lawford, D. R. Hose, *J. Med. Eng. Technol.* **2018**.

[51] H. J. Kim, I. E. Vignon-Clementel, J. S. Coogan, C. A. Figueroa, K. E. Jansen, C. A. Taylor, *Ann. Biomed. Eng.* **2010**.

[52] H. Tang, Z. Dai, M. Wang, B. Guo, S. Wang, J. Wen, T. Li, *J. Cardiovasc. Transl. Res.* **2020**.

[53] D. Burkhoff, M. S. Maurer, S. M. Joseph, J. G. Rogers, E. Y. Birati, J. E. Rame, S. J. Shah, *JACC Heart. Fail.* **2015**.

[54] L. S. Lilly, Ed. , *Pathophysiology of Heart Disease : A Collaborative Project of Medical Students and Faculty*, Wolters Kluwer/Lippincott Williams & Wilkins, Baltimore, MD, **2016**.

[55] S. G. Frangos, *Arch. Surg.* **1999**.

[56] M. M. Dua, R. L. Dalman, *Vascul. Pharmacol.* **2010**.

[57] B. A. Carabello, W. J. Paulus, *Lancet* **2009**.

[58] G. A. Fishbein, M. C. Fishbein, *Curr. Cardiol. Rep.* **2019**.

59] G. Koullias, R. Modak, M. Tranquilli, D. P. Korkolis, P. Barash, J. A. Elefteriades, *J. Thorac. Cardiovasc. Surg.* **2005**.

[60] Abaqus Dassault Systemes, **2008**.

[61] B. Baillargeon, N. Rebelo, D. D. Fox, R. L. Taylor, E. Kuhl, *Eur. J. Mech. A, Solids* **2014**, *48*, 38.

[62] P. P. Roeleveld, D. M. Axelrod, D. Klugman, M. B. Jones, N. K. Chanani, J. W. Rossano, J. M. Costello, *Cardiol. Young* **2018**.

[63] T. Y. Hsia, S. Khambadkone, A. N. Redington, F. Migliavacca, J. E. Deanfield, M. R. De Leval, *Circulation* **2000**.

[64] T. Y. Hsia, S. Khambadkone, J. E. Deanfield, J. F. N. Taylor, F. Migliavacca, M. R. De Leval, *J. Thorac. Cardiovasc. Surg.* **2001**.

[65] J. A. Feinstein, D. W. Benson, A. M. Dubin, M. S. Cohen, D. M. Maxey, W. T. Mahle, E. Pahl, J. Villafae, A. B. Bhatt, L. F. Peng, B. A. Johnson, A. L. Marsden, C. J. Daniels, N. A. Rudd, C. A. Caldarone, K. A. Mussatto, D. L. Morales, D. D. Ivy, J. W. Gaynor, J. S. Tweddell, B. J. Deal, A. K. Furck, G. L. Rosenthal, R. G. Ohye, N. S. Ghanayem, J. P. Cheatham, W. Tworetzky, G. R. Martin, *J. Am. Coll. Cardiol.* **2012**.

[66] D. D. Gabbert, C. Hart, M. Jerosch-Herold, P. Wegner, M. S. Ravesh, I. Voges, I. Kristo, A. A. L. Bulushi, J. Scheewe, A. Kheradvar, H. H. Kramer, C. Rickers, *Sci. Rep.* **2019**.

[67] S. M. Bradley, *Oper. Tech. Thorac. Cardiovasc. Surg.* **2006**.

[68] C. Singh, C. Wong, X. Wang, *J. Funct. Biomater.* **2015**.

[69] A. C. Egbe, H. M. Connolly, W. R. Miranda, N. M. Ammash, D. J. Hagler, G. R. Veldtman, B. A. Borlaug, *Circ. Hear. Fail.* **2017**.

[70] M. Horvath, D. Van Story, J. Hochstein, A. Pozo Alvarez, E. T. Roche, in *IEEE Int. Conf. Biomed. Robot. Biomechatronics*, **2020**.

[71] M. A. Horvath, L. Hu, T. Mueller, J. Hochstein, L. Rosalia, K. A. Hibbert, C. C. Hardin, E. T. Roche, *APL Bioeng.* **2020**.

[72] S. van Wyk, L. Prahl Wittberg, K. V Bulusu, L. Fuchs, M. W. Plesniak, *Phys. Fluids* **2015**, *27*, 71901.

[73] T. E. Carew, R. N. Vaishnav, D. J. Patel, *Circ. Res.* **1968**, *23*, 61.

[74] F. Cuomo, S. Roccabianca, D. Dillon-Murphy, N. Xiao, J. D. Humphrey, C. A. Figueroa, *PLoS One* **2017**.

[75] C. T. DOTTER, D. J. ROBERTS, I. STEINBERG, *Circulation* **1950**, *2*, 915.

[76] S. K. Sonavane, D. M. Milner, S. P. Singh, A. K. Abdel Aal, K. S. Shahir, A. Chaturvedi, *Radiographics* **2015**.

[77] S. Patil, S. Jadhav, N. Shetty, J. Kharge, B. Puttegowda, R. Ramalingam, M. N. Cholenahally, *Indian Heart J.* **2016**, *68 Suppl 3*, S26.

[78] S. K. Ghosh, S. Paul, *Surg. Radiol. Anat.* **2012**.

[79] G. Mozes, P. Gloviczki, in (Ed.: J.J.B.T. Bergan), Academic Press, Burlington, **2007**, pp. 15–25.

[80] A. González-Mansilla, P. Martinez-Legazpi, A. Prieto, E. Gomá, P. Haurigot, C. Pérez del Villar, V. Cuadrado, A. Delgado-Montero, R. Prieto, T. Mombiela, E. Pérez-David, E. Rodríguez González, Y. Benito, R. Yotti, M. Pérez-Vallina, F. Fernández-Avilés, J. Bermejo, *Heart* **2019**, *105*, 911 LP.

[81] S. B. Capps, R. C. Elkins, D. M. Fronk, *J. Thorac. Cardiovasc. Surg.* **2000**, *119*, 975.

[82] T. Soeki, N. Fukuda, H. Shinohara, K. Sakabe, Y. Onose, Y. Sawada, Y. Tamura, *Eur. J. Echocardiogr. J. Work. Gr. Echocardiogr. Eur. Soc. Cardiol.* **2002**, *3*, 128.

[83] A. Bhatia, *Ann. Card. Anaesth.* **2016**, *19*, S21.

[84] B. D. Hoit, R. A. Walsh, in *Hurst's Hear. 13e*, **2011**.

[85] M. A. Gangemi, *Pathophysiology of Heart Disease*, **1995**.

[86] A. M. Maceira, S. K. Prasad, M. Khan, D. J. Pennell, *J. Cardiovasc. Magn. Reson.* **2006**.

[87] A. M. Maceira, S. K. Prasad, M. Khan, D. J. Pennell, *Eur. Heart J.* **2006**.

[88] P. Kligfield, *Heart Disease: A Textbook of Cardiovascular Medicine, Philadelphia*, **1998**.

[89] E. Aune, M. Baekkevar, J. Roislien, O. Rodevand, J. E. Otterstad, *Eur. J. Echocardiogr.* **2009**.

[90] S. Magder, F. Bafaqeeh, *J. Intensive Care Med.* **2007**, *22*, 44.

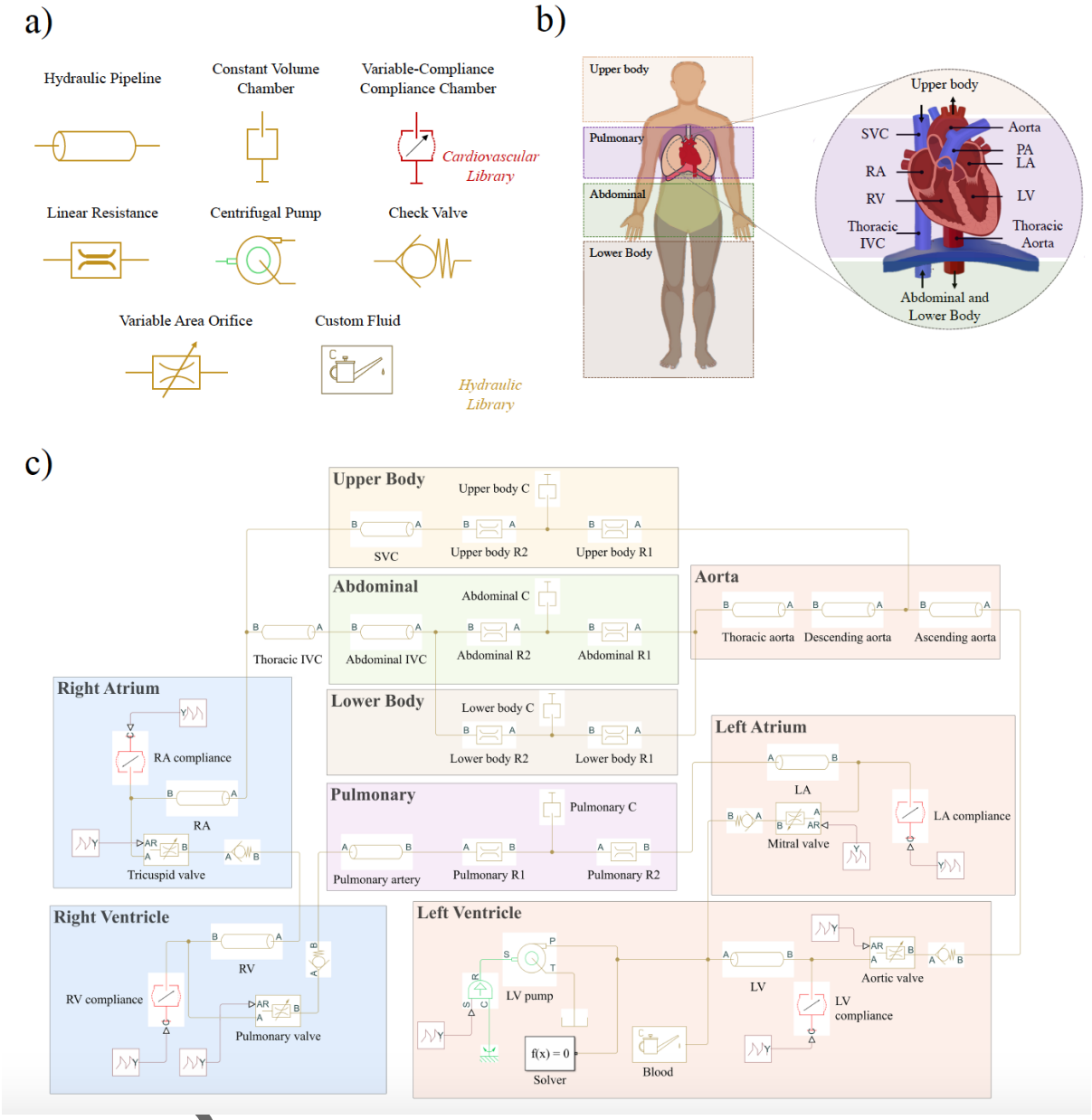

Figure 1: a) Simulation elements from the SIMSCAPE default *Hydraulic* library and the custom *Cardiovascular* library. b) Representation of the cardiovascular system anatomy divided into the upper body, pulmonary, abdominal and lower body circulations. c) Schematic of the simulation based on the human anatomy.

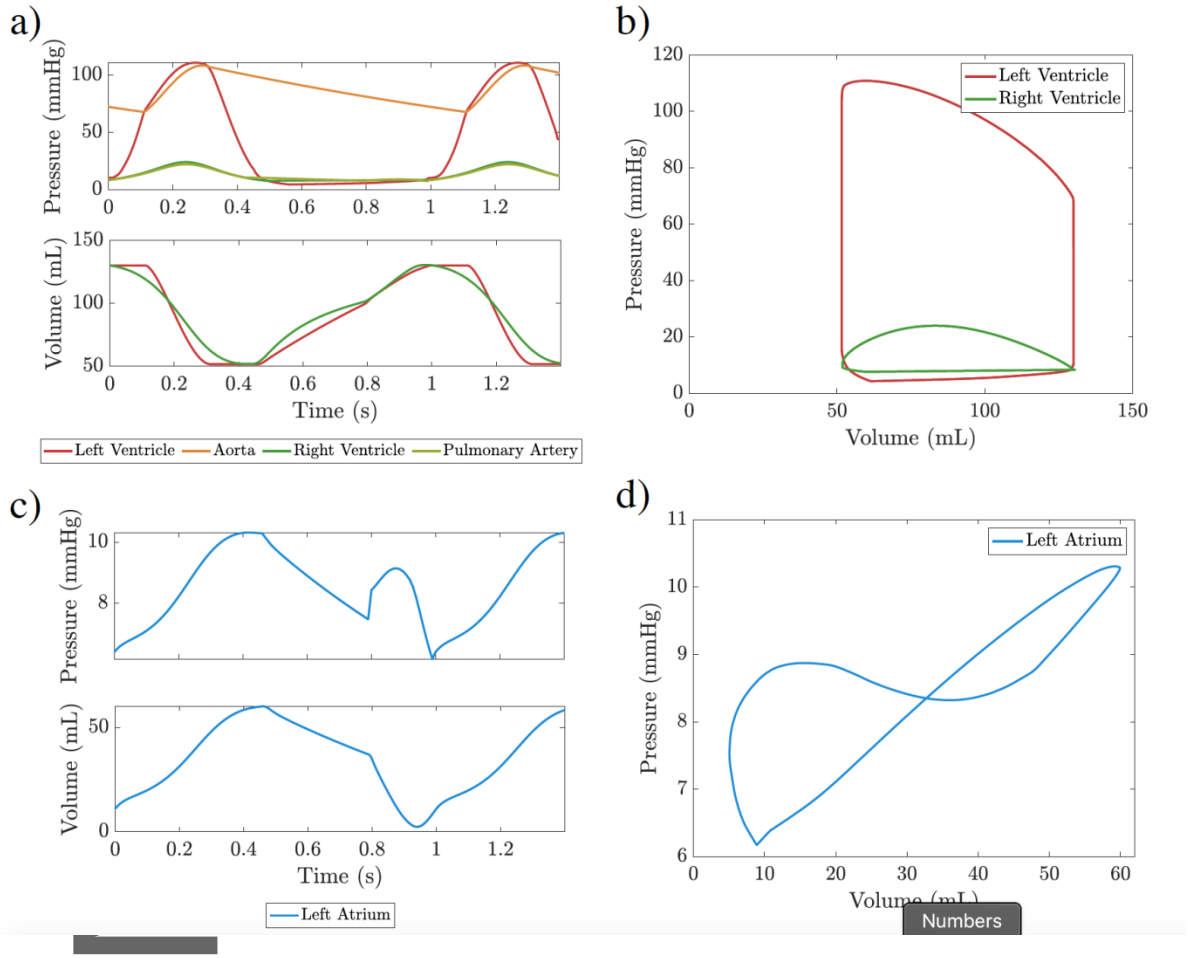

Figure 2: Cardiovascular hemodynamics results. a) Pressure and volume tracings of the left ventricle, aorta, right ventricle, and pulmonary artery. b) PV loop of the left and right ventricles. c) Pressure and volume tracings of the left atrium. d) PV loop of the left atrium.

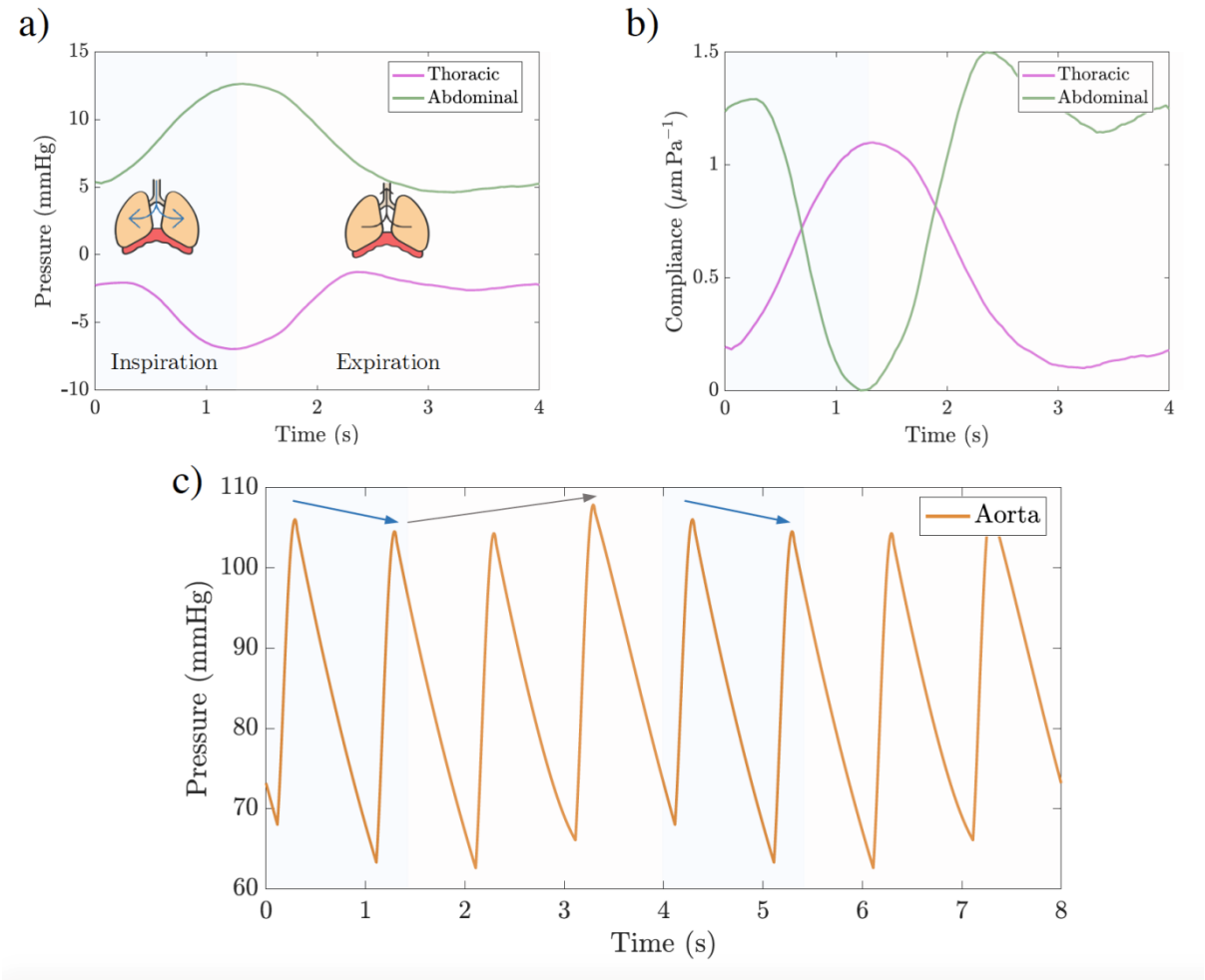

Figure 3: a) Thoracic and abdominal pressures during the breathing cycle. b) Estimated thoracic and abdominal vascular compliances during the breathing cycle. c) Effects of respiratory mechanics on aortic pressure.

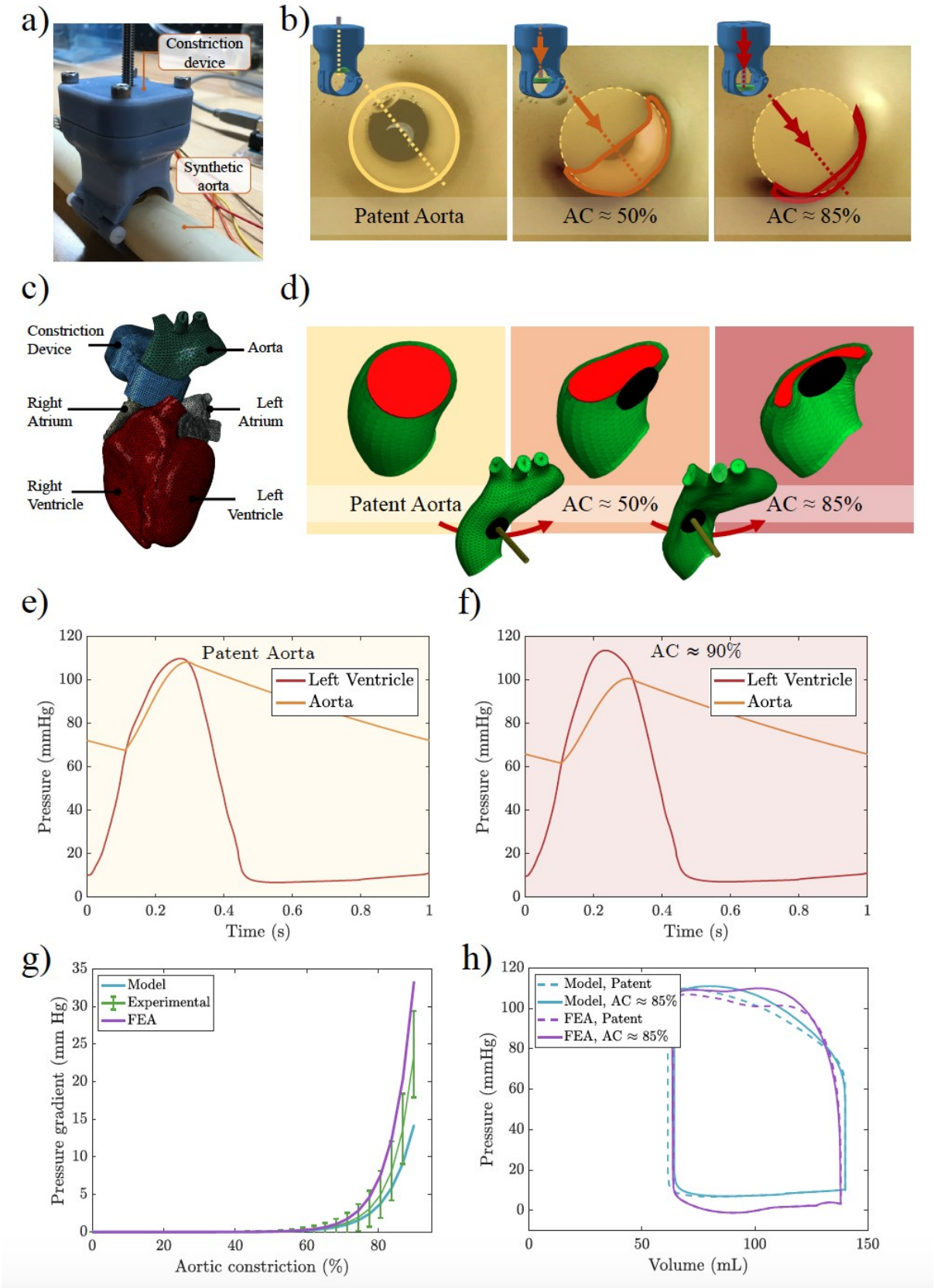

Figure 4: a) Experimental set-up showing the electromechanical constriction device on the synthetic aorta. b) Images recorded by an endoscopic camera inserted in the flow loop, showing cross-sectional variations of the aorta at AC ≈ 0%, 50%, 85%. c) FEA set-up illustrating the constriction device on the aortic wall. d) Cross-sectional variations of the aorta at AC ≈ 0%, 50%, 85% obtained on the FEA simulation. Pressure tracings of the left ventricle and aorta for e) the patent aorta and f) AC ≈ 90%. g) Changes in transaortic pressure gradient with cross-sectional aortic constriction obtained by our model (R^2 = 0.8965), *in vitro* (R^2 = 0.9788 ± 0.0027, N = 3), and on FEA (R^2 = 0.8875). h) PV loops of the left ventricle computed by our model and via FEA at AC ≈ 0%, 85%.

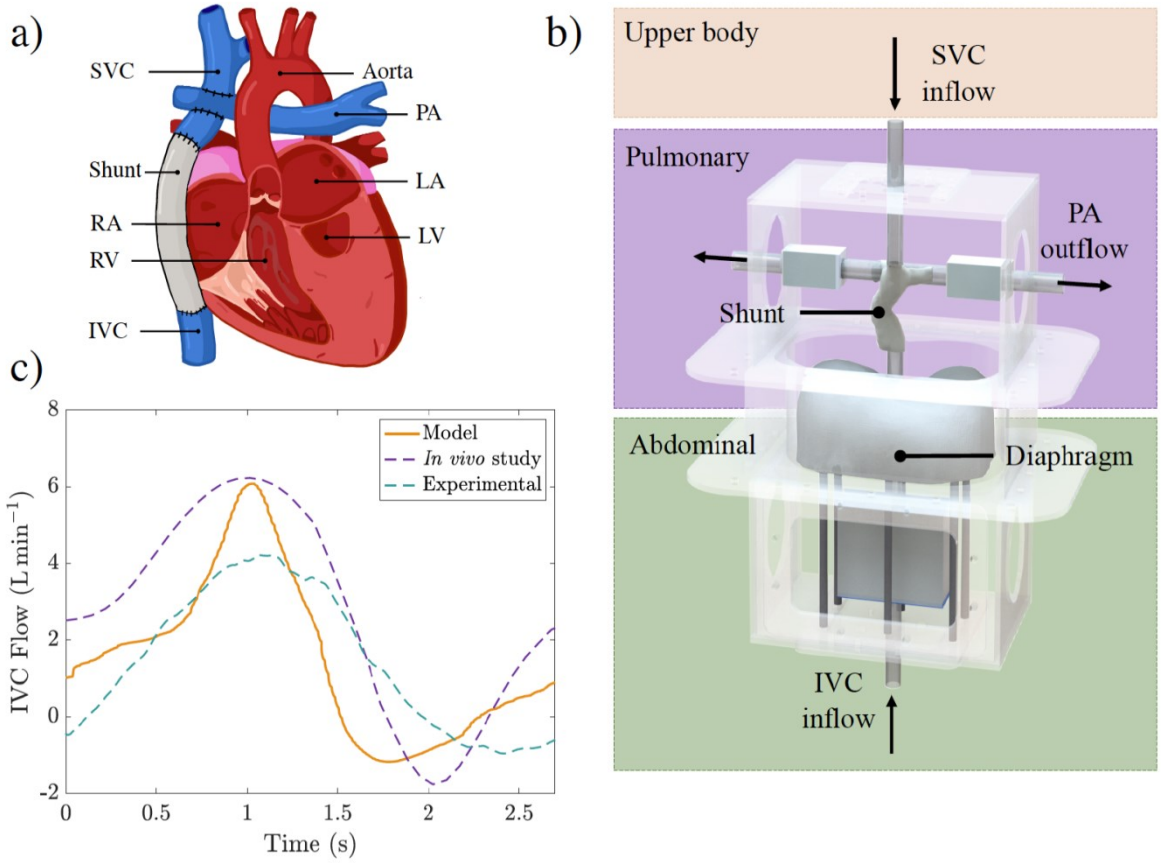

Figure 5: a) Representation of the Fontan anatomy. b) Schematic of the benchtop simulator used for validation. c) Comparison of Fontan hemodynamics across our *in silico* model, *in vitro* platforms and *in vivo* study,[66] showing the characteristic low pulsatile flow within the IVC.

Table 1. Parameters of baseline simulation.

	Density [kg m^{-3}]	Kinematic viscosity [mm^2 s^{-1}]	Bulk modulus [GPa]
Blood	1060[72]	3.55[72]	2.2[73]
	Diameter [cm]	**Length [cm]**	**Compliance [m Pa^{-1}]**
Left ventricle	4.4[60]	7[60]	0.02 – 8 10^{-7}
Right ventricle	4.8[60]	5[60]	1.8 – 5.5 10^{-5}
Left atrium	5[60]	7.5[60]	0.8 – 1.7 10^{-5}
Right atrium	5.6[60]	5[60]	1.9 – 2.3 10^{-5}
Ascending aorta	2.65[74]	8.8[74]	4.5 10^{-7}
Descending aorta	2.15[74]	6.9[74]	7.0 10^{-7}
Thoracic aorta	1.92[74]	33.2[75]	1.7 10^{-7}
Pulmonary artery	3[60]	5[60]	2.2 10^{-7}
SVC[a)]	2.1[76]	7.1[76]	5.0 10^{-6}
Abdominal IVC[b)]	1.4[77]	17[78]	4.4 10^{-6}

Thoracic IVC	1.4[77]	2.5[79]	6.4 10^{-7}
	Area [cm^2]		
Aortic valve	4[80]		
Pulmonary valve	5[81]		
Mitral valve	4.2[82]		
Tricuspid valve	5[83]		
	Resistance[c)] [Pa s m^{-3}]	Volume[d)] [L]	Compliance[d)] [m Pa^{-1}]
Upper body	0.31 – 5.2 10^{8}[22]	0.89[22]	6.7 10^{-8}[22]
Abdominal	0.15 – 2.3 10^{8}[22]	2.02[22]	3.6 10^{-8}[22]
Lower body	0.40 – 4.7 10^{8}[22]	0.51[22]	4.1 10^{-8}[22]
Pulmonary	0.50 – 5.0 10^{6} [54]	0.55[22]	6 10^{-7}[22]

[a)]Superior Vena Cava; [b)]Inferior Vena Cava; [c)]The two values in range refer to the venous and the arterial resistance respectively; [d)]Estimated from citation.

Table 2. Comparison of simulated hemodynamics with physiological range.

Parameter	Simulation	Physiology
Cardiac output [L min^{-1}]	4.7	4.4 – 7.1[84]
Stroke volume [mL]	79	51 – 111[84]
LV pressure [mmHg]		
Systolic	111	100 – 140[85]
Diastolic	4	3 – 12[85]
LV volume [mL]		
Systolic	51	37 – 57[86]
Diastolic	130	121 – 163[86]
Arterial pressure [mmHg]		
Systolic	108	100 – 140[85]
Diastolic	68	60 – 90[85]
RV pressure [mmHg]		
Systolic	24	15 – 30[85]
Diastolic	7	2 – 8[85]

RV volume [mL]		
Systolic	52	36 – 64[87]
Diastolic	130	121 – 167[87]
Pulmonary artery pressure [mmHg]		
Systolic	22	15 – 30[85]
Diastolic	7	4 – 12[85]
PCWP[a] [mmHg]	6 – 10	4 – 12[88]
LA volume [mL]	8 – 60	8 – 78[89]
CVP[b] [mmHg]	8 – 9	2 – 10[90]
RA volume [mL]	9 – 41	8 – 89[89]

[a]Pulmonary Capillary Wedge Pressure; [b]Central Venous Pressure

Table 3. Comparison of IVC hemodynamics across *in silico*, *in vitro*, and *in vivo* studies.

Parameter	Simulation	Experimental	*In vivo* study[66]
Respiratory rate [min^{-1}]	21.7	21.7	21.8 ± 4.3
Cardiac output [$L\ min^{-1}$]	2.0	2.2	1.9 ± 0.7

IVC pressure [mm Hg]	18.5	16.4	N.R.[a)]
IVC peak flow [L min^{-1}]	6.1	4.2	6.2

[a)]Not Reported

TOC

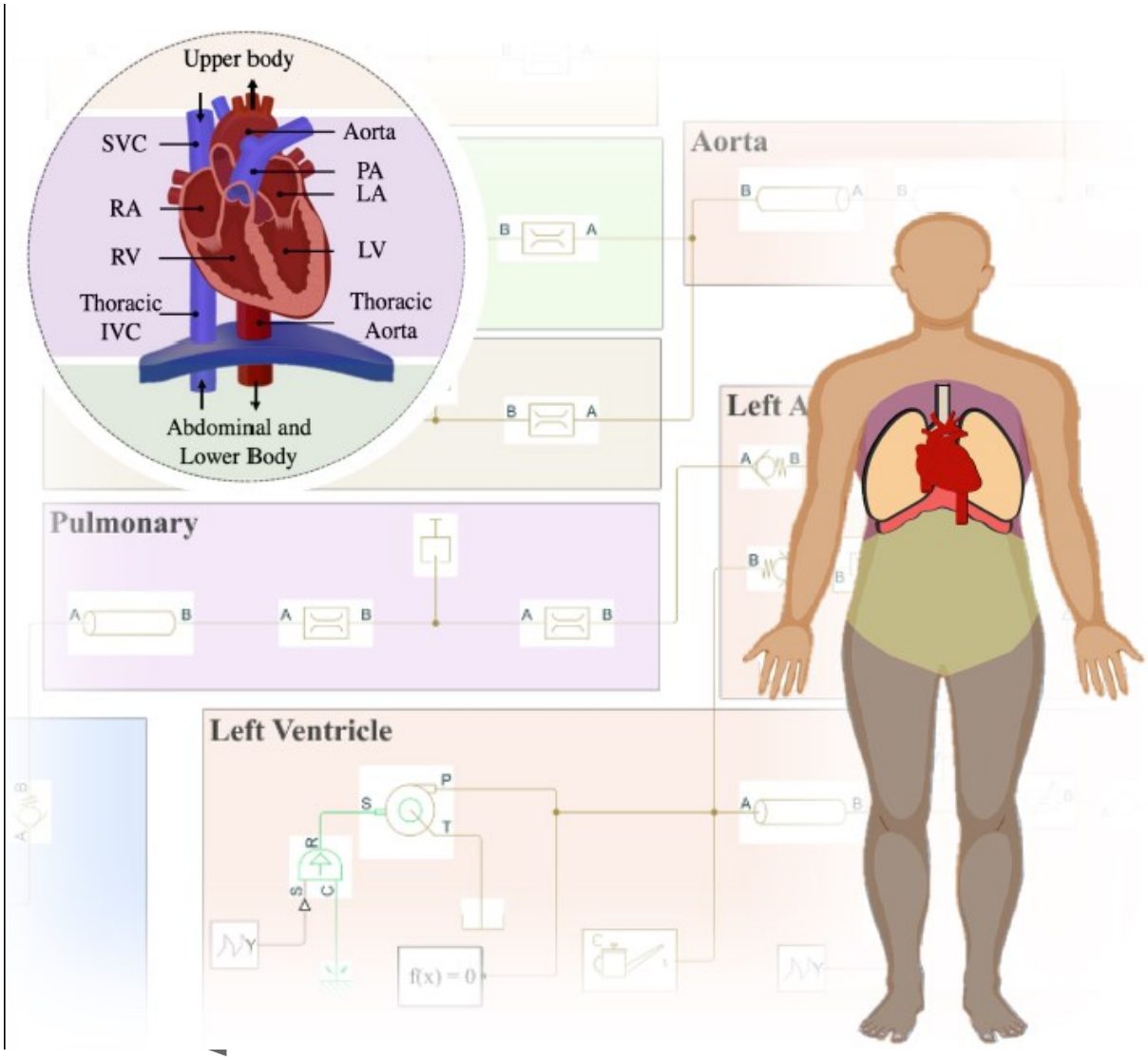

A lumped-parameter model of the cardiovascular system is developed to determine cardiovascular hemodynamics from hydraulic parameters in physiological and pathophysiological conditions, including left ventricular pressure overload and single-ventricle physiology. This provides a practical tool for the simulation of complex circulatory loops, optimization of medical interventions, and prediction of patient-specific hemodynamics of clinical relevance.